ADVANCED FUNCTIONAL MATERIALS
www.afm-journal.de

Oscillating-to-Continuous Combustion Transition in Mesoparticle Composites Through Manipulation of Heat Feedback

*Yujie Wang, Mahbub Chowdhury, Yuxin Zhou, George Issac Paul, Keren Shi, and Michael R. Zachariah**

In this study, free-standing composites consisting of 90 wt% nanoenergetic mesoparticles are fabricated and their combustion characteristics are investigated. The findings reveal that the integrity of the mesoparticles remains intact during the printing process and a reduction in sintering is observed for the composite of mesoparticles compared to the physical mixture. However, the composite of mesoparticles exhibits noncontinuous and oscillating propagation behavior at a steady frequency of ≈5 Hz. This is attributed to insufficient heat feedback from the flame to the unburnt material. To address this issue, carbon fiber (C.F.) is introduced into the composite to enhance heat feedback to the reaction front by intercepting hot agglomerates near the burning surface. Incorporating C.F. leads to steady propagation of the composite. Agglomerate residence time and characteristic heat transfer time analysis near the burning surface indicate that while the composite without C.F. has agglomerate residence time on the same order of magnitude as the characteristic heat transfer time, the composite with C.F. has significantly increased overall agglomerate residence time compared to the characteristic heat transfer time. This confirms the enhanced heat feedback through C.F. inclusion. This study demonstrates the crucial role of heat feedback in the combustion behavior of energetic composites.

1. Introduction

The use of nanostructures has significantly increased the research activity into novel classes of energetic materials.[1–8] The reactivity of thermites that typically composed of metals and metal oxides has been increased significantly through the utilization of nanoscale particles.[9] The enhanced reactivity is generally attributed to the increased specific surface area and decreased diffusion length scale of nanoparticles.[1] Aluminum (Al) particles are widely used as additives in energetic materials such as explosives, propellants, and pyrotechnics to improve combustion performance due to their high energy density, availability, and low cost.[10–13] Nevertheless, substituting micron-scale aluminum with nanoscale aluminum (nAl) in energetic materials results in combustion rates that are lower than theoretically expected,[4,14] as well as more difficult formulation and processing. This former is attributed to the agglomeration/sintering that results in loss of nanostructure during combustion, as nAl tends to aggregate, sinter, and coalesce.[15] Agglomeration negates the benefits of using nAl and reduces the rate of energy release.[11,14,16–22]

We have explored an approach to minimize sintering effects as well as some of the processing constraints in working with nanomaterials in formulations through the creation of mesoparticles. A mesoparticle is an assembly of nanometric metal fuels along with an optional oxidizer, and very importantly a low-temperature gas generator/binder. This type of particle system, which assembles nanomaterials into supermicron particles, has been demonstrated to yield considerable improvement in combustion performance on a particle combustion level.[13,23–25] The enhanced reactivity is attributed to the breaking up of soft agglomerates before/during combustion from the low-temperature gas generation of nitrocellulose (NC) as well as better mixing between fuel and oxidizer. Another crucial advantage of mesoparticles is their ability to maintain an internal surface area roughly equivalent to the specific surface area of a nanoparticle while providing ease of processing for high-loading solid propellant fabrication.[23] The high specific surface area of nAl results in severe processing challenges as the integration of nAl into polymer binders leads to dramatically increased viscosity. By assembling nAl into mesoparticles, the overall particle surface area decreases significantly, resulting in easier processing and higher particle loading of solid propellants.[26] Despite the potential advantages of utilizing mesoparticles in energetic materials, an investigation focusing on the combustion characteristics of a solid composite with high mesoparticle loading is still lacking and is the motivation of this paper.

Y. Wang, M. Chowdhury, Y. Zhou, G. Issac Paul, K. Shi, M. R. Zachariah
University of California Riverside
900 University Avenue, Riverside, CA 92521, USA
E-mail: mrz@engr.ucr.edu

The ORCID identification number(s) for the author(s) of this article can be found under https://doi.org/10.1002/adfm.202406722

DOI: 10.1002/adfm.202406722

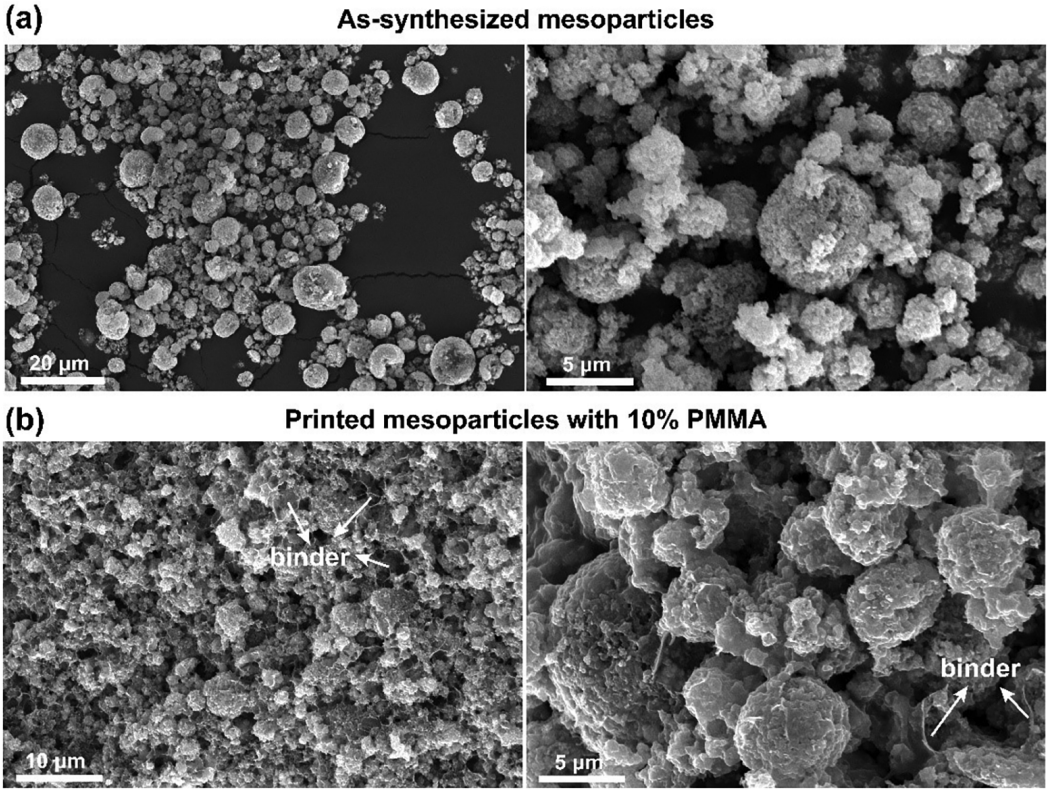

Figure 1. SEM images of as-synthesized mesoparticles from the spray-drying process a) and the mesoparticles incorporated into the printed composite b). Note: The binder labeled in (b) refers to the binder used for printing (PMMA).

In this study, we fabricated free-standing composites consisting of mesoparticles at a 90% loading using 3D printing and compared their combustion behaviors with composites made from a physical mixture. Scanning Electron Microscopy (SEM) analysis of the printed composite confirmed that the integrity of the mesoparticles was preserved throughout the printing process. High-speed microscopic and macroscopic imaging techniques were utilized to study the combustion behavior of the printed composites. Microscopic imaging revealed reduced sintering in the composite of mesoparticles compared to the physical mixture composite during combustion. However, macroscopic imaging showed that while the physical mixture composite propagated steadily, the mesoparticle composite exhibited non-continuous and periodic propagation behavior. This behavior is attributed to insufficient heat feedback from the flame to the unburnt region, hindering steady propagation. To address this issue, carbon fiber was incorporated into the mesoparticle composite to enhance heat feedback.[27,28] Microscopic imaging demonstrated that carbon fiber intercepted agglomerates near the burning surface, while macroscopic imaging revealed that the mesoparticle composite with carbon fiber propagated steadily. Theoretical calculations were performed to compare the residence time of agglomerates and the characteristic heat transfer time near the burning surface. These calculations confirm the critical role of heat feedback in the propagation of the composite of mesoparticles.

2. Results and Discussion

The concept of utilizing mesoparticles implies that it is crucial to ensure the mesoparticles maintain their integrity throughout the printing process. As shown in **Figure** 1a,b, there is no apparent difference in morphology between the mesoparticles (Al-CuO-7.5 wt% NC) synthesized through the spray-drying process and those incorporated into the printed composite. This confirms that the mesoparticles remain intact during the printing process.

Combustion characteristics of the printed composites of the physical mixture and mesoparticles were investigated with high-speed macroscopic imaging. It was expected that the printed composite of mesoparticles has a higher burn rate than that of a physical mixture due to the higher intrinsic reactivity of mesoparticles compared to a physical mixture, as previously demonstrated.[23,25] **Figure** 2a displays a series of time-resolved macroscopic snapshots of the physically mixed composite burning. However, the composite of mesoparticles displays non-continuous propagation behavior that reduces the overall burn rate significantly, resulting in a considerably lower macroscopic burn rate than the physically mixed composite (Figure 2b). Furthermore and very curiously, the light intensity extracted from the macroscopic imaging video demonstrates a periodic (but steady) combustion characteristic (blinking) during propagation of the mesoparticle composite (Figure S1, Supporting Information each peak represents a visible combustion event). The time interval between two adjacent visible (blinking) combustion

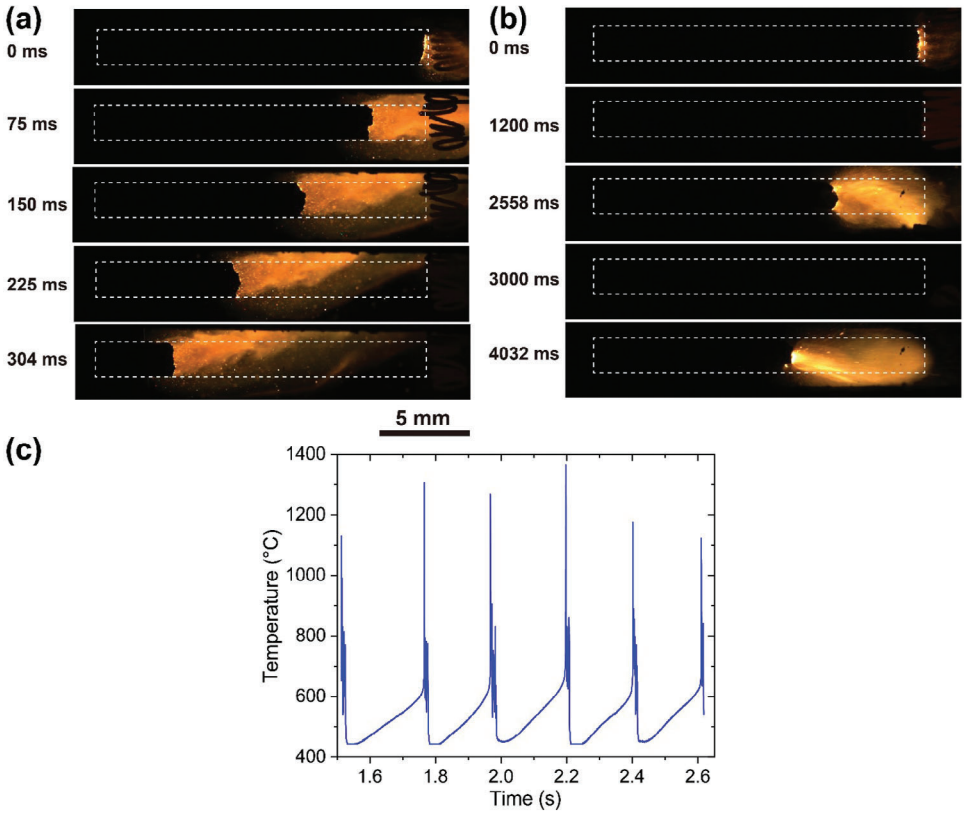

Figure 2. Time-resolved snapshots from high-speed macroscopic video of physical mixture composite a) and mesoparticle composite (b). Note: The dashed lines represent the printed composites before ignition. Time-resolved temperature from the IR imaging video for the composite of mesoparticles showing periodic combustion (c).

events is ≈200 ms and the burn time of each combustion event is ≈15 ms, which appears to be quite consistent.

The fact that the composite of mesoparticles reignites after a combustion event followed by a relatively long period of time without any visible flame suggests the presence of a different ignition source. IR imaging was utilized to measure temperature in-between of the visible combustion events for the composite of mesoparticles and the result is displayed in Figure 2c. The sharp peaks in Figure 2c correspond to the visible thermal events shown in Figure S1 (Supporting Information). Sample temperature drops to ≈450 °C abruptly at the end of a combustion event, and then gradually increases to ≈650 °C, which is approximately the ignition temperature of Al/CuO composite measured from our previous study.[11] Once this temperature is reached, the sample is reignited and another combustion event occurs. This behavior will be discussed in more detail in the following section, as well as how to mitigate this behavior.

The preceding analysis primarily focuses on how the non-continuous propagation of the composite of mesoparticles occurs but does not address the reason why the utilization of mesoparticles results in such a combustion characteristic. High-speed microscopic imaging facilitates direct observation of events occurring near the flame front, providing valuable insights into the combustion behavior of a thermite reaction. **Figure** 3a,b displays the representative snapshots taken from the high-speed microscopic videos for the composite of the physical mixture and the composite of mesoparticles, respectively. While previous studies have used ex-situ techniques to prove the reduction in sintering when assembling Al/CuO into mesoparticles,[23,25] the microscopic videos in the current study enable in situ observation of the reduced sintering of mesoparticle over the physical mixture. SEM was utilized to analyze the post-combustion products for the composites with physical mixture and mesoparticles, as displayed in Figure 3c,d, respectively. It is evident that the composite with mesoparticles produces smaller agglomerates during combustion compared to the composite with the physical mixture, consistent with the observation from microscopic imaging.

Steady propagation of an energetic system necessitates sufficient transfer of heat from the reaction front or flame to the unreacted material.[29–33] Previous studies on Al/CuO mesoparticles with NC as the binder has demonstrated that the higher reactivity from mesoparticles arises from the reduced sintering as a result of significant gas generation from NC. However, for the composite with mesoparticles, the large amount of gas generation from NC appears to lead to the rapid departure of agglomerates from the burning surface, resulting in less conductive heat feedback to the unburnt region compared to the composite with a physical mixture. This low heat feedback leads to the extinguishment of a combustion event observed from the macroscopic imaging. It is noteworthy that the composite comprises 10% polymer (PMMA) to bind mesoparticles into a free-standing stick through 3D printing, and PMMA undergoes

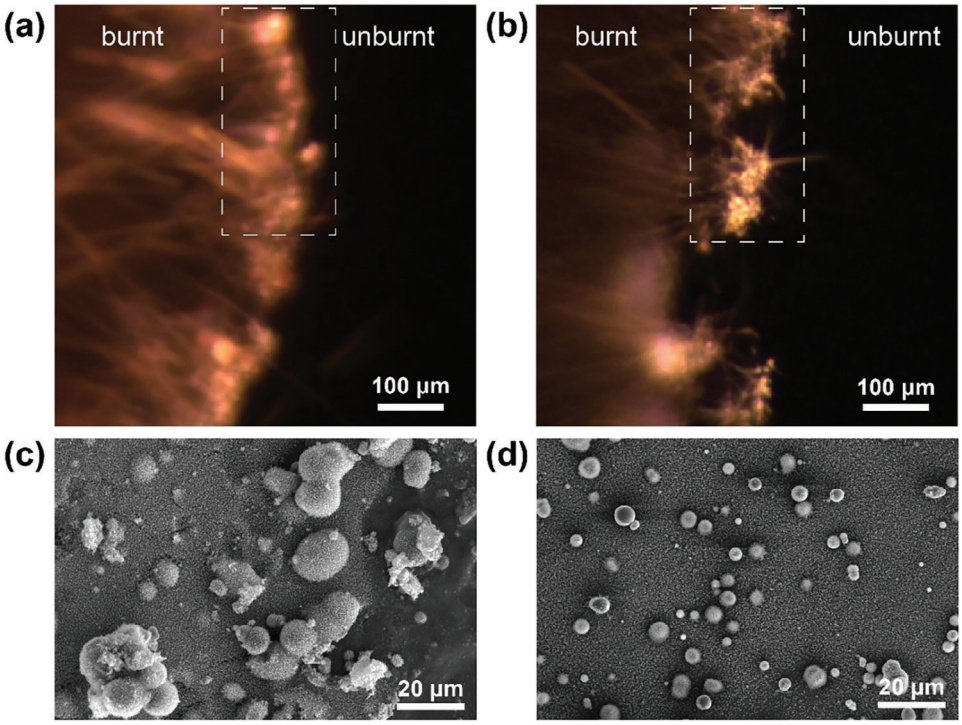

Figure 3. Snapshots from high-speed microscopic video for the combustion of the composites of physical mixture a), and mesoparticles b). The dashed lines show the representative combustion characteristics on the burning surface. SEM images of the post-combustion product from the composites of physical mixture c), and mesoparticles d), i.e., mesoparticle combustion products are smaller.

combustion alongside the mesoparticles.[34,35] However, the flame of PMMA is not visible in the color camera with the settings to observe burning agglomerates, as the combustion products of PMMA (mainly CO_2, CO, H_2O[36,37]) primarily emit in the infrared range.[38,39] After a combustion event, observed from the macroscopic camera, PMMA continues to combust, but more slowly and the heat generated increases the local temperature sufficiently to ignite nearby mesoparticles, thus resulting in another mesoparticle transient event. This is supported by the IR imaging result displayed in Figure 2c. The ignition of these mesoparticles initiates a new combustion event observed from the macroscopic camera. This series of events repeats, resulting in the non-continuous and cyclic combustion behavior observed in the composite of mesoparticles. To reinforce this point, a composite comprising 20% PMMA and 80% mesoparticles, i.e., less mesoparticles also exhibits a non-continuous and cyclic propagation behavior. However, the time interval between two adjacent combustion events is reduced by almost a half to ≈110 ms. This discrepancy is attributed to the higher content of PMMA in the composite, leading to a faster accumulation of heat from the PMMA flame and consequently resulting in quicker reignition of the composite. A more extensive investigation into this phenomenon is currently underway in our research group.

So far, we have conjectured that insufficient heat feedback causes the non-continuous propagation of the composite of mesoparticles. A primary question now arises: If indeed this is a heat feedback issue, then would increasing heat feedback result in continuous propagation for the composite of mesoparticles? Previous studies have demonstrated that adding carbon fiber (C.F.) increases heat feedback of a solid-state composite by capturing the agglomerates departed from the burning surface.[27,28] Inspired by these studies, we incorporate 2 wt% of C.F. in the 3D printed composite of mesoparticles to increase the heat feedback (4% PMMA and 6% HPMC as the binder as discussed in Section 2.3). For simplicity, this composite will be referred to as mesoparticle-2% C.F. composite in the following discussion. Mesoparticle composites with 4% PMMA and 6% HPMC as the binder and no C.F. was also prepared and used for comparison in the following analysis. High-speed macroscopic and microscopic imaging reveals that the composite with no C.F. cannot propagate while the mesoparticle-2% C.F. composite has continuous propagation. **Figure** 4a demonstrates stable and linear propagation of the mesoparticle-2% C.F. composite. Microscopic imaging reveals that carbon fibers intercept burning agglomerates, causing them to remain near the burning surface rather than dispersing to a greater distance, as shown in Figure 4b. Temperature measurements from three-color pyrometry indicate that the agglomerates on the C.F. maintain a temperature of ≈2100 K when they are within a distance of ≈1 mm from the burning surface. Our recent molecular dynamic simulation work.[40] found that the intercepted Al agglomerates would form Al—C bonds with the surface of carbon fibers to enhance their binding. Agglomerates on the burning surface and those have recently departed from the burning surface without being intercepted by the carbon fibers have a temperature of ≈2700 K, which is close to the adiabatic flame temperature of Al/CuO at 2840 K.[11] Notably, the temperature of the agglomerates on the

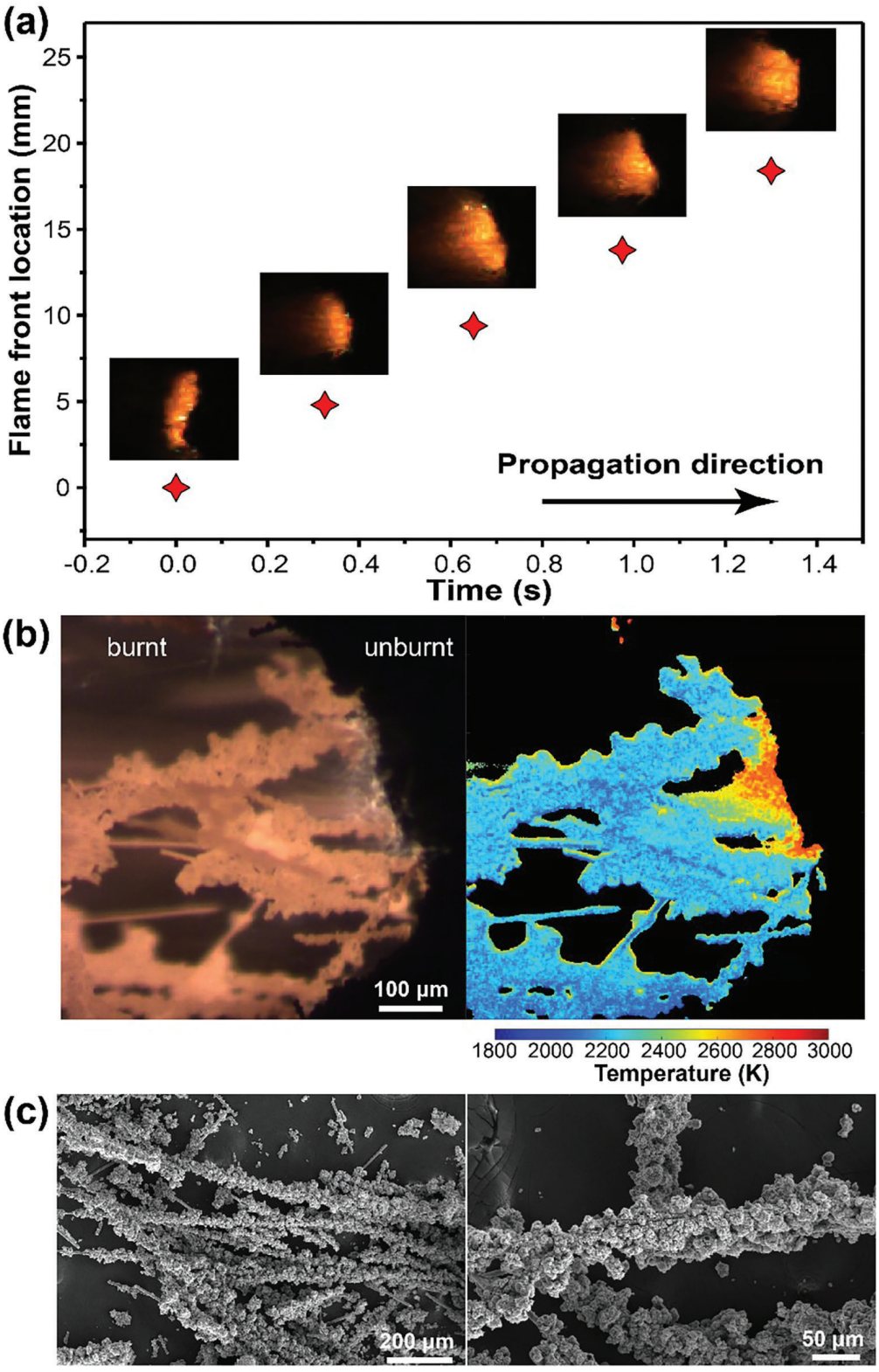

Figure 4. Time-resolved flame front position with a corresponding snapshot from macroscopic imaging for the composite of mesoparticles with 2% C.F.a). Representative snapshot from high-speed microscopic video and its corresponding temperature map from three-color pyrometry b) and SEM images of the post-combustion product c) for the composite of mesoparticles with 2% C.F.

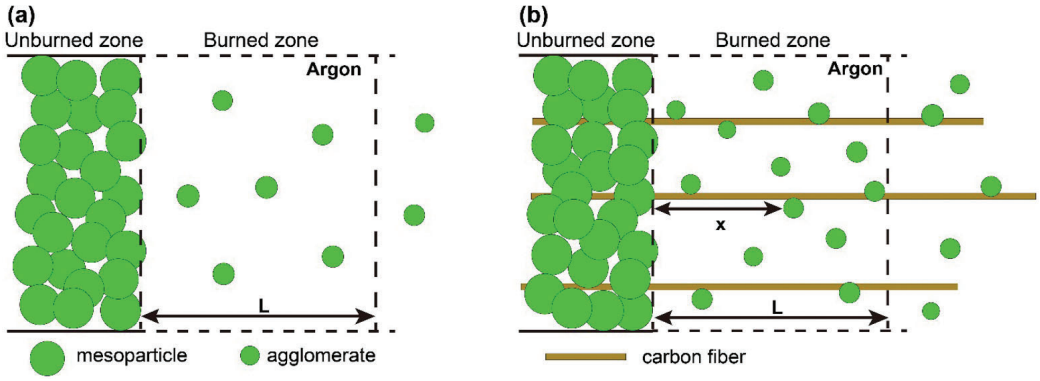

Figure 5. Illustration depicting the region near the burning surface for the composite of mesoparticles without C.F. a) and with C.F. (b).

burning surface of the mesoparticle composite without C.F. is also ≈2700 K (Figure S2, Supporting Information), indicating that the addition of C.F. has minimal impact on the temperature of the agglomerates. The lower temperature of agglomerates on the C.F. compared to those not on the C.F. can be attributed to their rapid heat loss to the C.F. with high thermal conductivity. SEM images of the post-combustion product of the mesoparticle-2% C.F. composite displayed in Figure 4c show the extensive attachment of agglomerates on the carbon fibers, consistent with the observation from microscopic imaging (Figure 4b).

Previous studies have demonstrated that heat feedback plays a crucial role in the propagation of an energetic material as steady propagation necessities sufficient heat from the flame to the unreacted material.[29–32] The preceding analysis has demonstrated qualitatively that increasing heat feedback of the composite of mesoparticles by incorporating carbon fiber results in a continuous and stable propagation. Now, let us perform a semi-quantitative analysis on the change in heat feedback resulting from the incorporation of carbon fiber by comparing the agglomerate residence time (t_{res}) and characteristic heat transfer time ($t_{heat\ transfer}$) in a region near the burning surface. Agglomerate residence time refers to the time needed for an agglomerate to travel a given distance immediately after departing from the burning surface. We start by simplifying the system to one dimension and building a control distance close to the burning surface, within which heat transferred from the agglomerates is considered (**Figure 5**). The length of the control distance L was varied from 50 to 200 μm as it is in between the mesoparticle size (≈3 μm) and the C.F. length (≈3 mm). For this analysis the results were not found to change significantly over this range of L. Convective heat feedback is neglected as the combustion test was conducted within a largely unconfined environment (the combustion chamber has a cross-section area 4 orders of magnitude higher than that of the composite) and the hot gas and particles unlikely move backward to the unburn material.[32] Radiative heat transfer is also neglected as the presence of C.F. should have minimal impact on the radiative property of agglomerates. Therefore, heat transfer time ($t_{heat\ transfer}$) is simplified to heat conduction time (t_{cond}) hereafter. Agglomerate residence time for the composite with bare mesoparticles is represented by Equation (1). For the mesoparticle-2% C.F. composite, there are two classes of agglomerates: those that are not intercepted by C.F. (Equation 1), and those that are intercepted by C.F. (Equation 2).

$$t_{res1} = \frac{L}{v_x} \tag{1}$$

$$t_{res2} = \frac{L - x}{u} \tag{2}$$

where x is the distance from the agglomerate to the burning surface, v_x is the measured agglomerate speed within L, u is the macroscopic burn rate of the mesoparticle-2% C.F. composite (1.5 cm s^{-1}), t_{res1} is the residence time of the agglomerate that is not intercepted by C.F., and t_{res2} is the residence time of the agglomerate that is intercepted by C.F. The values of x and v_x are obtained from high-speed microscopic imaging by tracking the traveling time and distance after the detachment of the agglomerate from the burning surface. More details about estimating agglomerate residence time can be found in the Supporting Information.

For an order-of-magnitude estimate of heat conduction time (t_{cond}), we assume that the gas medium near the burning surface is argon and there is no interaction among agglomerates. The heat conduction time is defined by Equation (3).[41]

$$t_{cond} \sim \frac{L^2}{\alpha} \tag{3}$$

where α is the thermal diffusivity of the medium (Ar or C.F) obtained by Equation (4).

$$\alpha \sim \frac{k}{\rho c_p} \tag{4}$$

where k is the thermal conductivity, ρ is the density, and c_p is the heat capacity. For the composite without C.F., argon is the only heat-conduction medium. The density of argon is calculated based on the ideal gas law, and the thermal conductivity and heat capacity of argon are calculated with USC Mech II.[42] For the composite with C.F., there are two scenarios for the agglomerates to conduct heat back to the unburnt composite: those that are not intercepted by C.F., and those that are intercepted by C.F. (Figure 5). It is assumed that the agglomerates not intercepted by C.F. conduct heat through argon only and agglomerates intercepted by C.F. conduct heat through C.F. only. The thermal

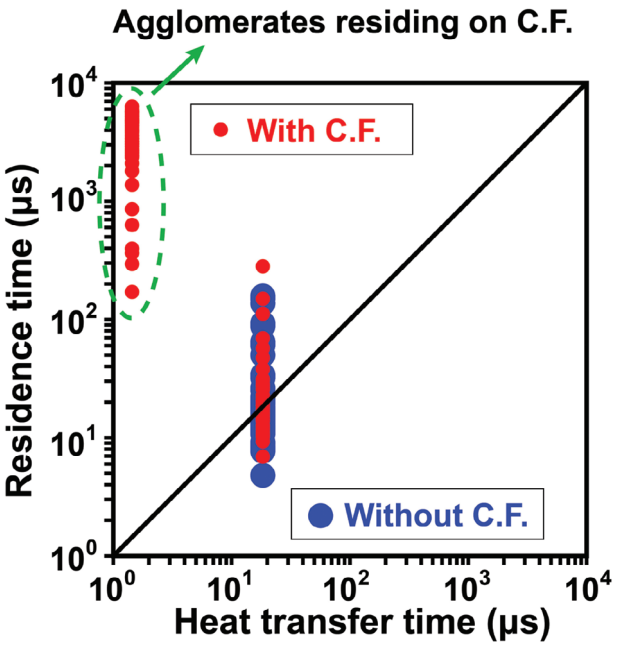

Figure 6. Estimated agglomerate residence time and characteristic heat transfer time for the composite of mesoparticles with and without C.F. Note: Each symbol represents a measured particle. The diagonal is there to aid the reader and represents the condition where: "heat transfer characteristic time ≈ agglomerate residence time".

conductivity of C.F. used in the current study is estimated to be 10 W m^{-1} K^{-1} and the density and heat capacity of C.F. used are based on a previous study.[27]

Figure 6 illustrates the estimated agglomerate residence time and characteristic heat transfer time in the region ($L = 100\ um$) near the burning surface for the composites of mesoparticles with and without C.F. Other cases with varying L can be found in the supplemental. In the case of the composite without C.F., the majority of the estimated residence time is on the same order of magnitude as the heat transfer time. However, for the composite with C.F., in addition to the agglomerates having residence time on the same order of magnitude as the heat transfer time, the agglomerates intercepted by the C.F. demonstrate residence times three orders of magnitude higher than the heat transfer time. This quantitatively confirms the significant increase in heat feedback resulting from the inclusion of C.F. Such enhanced heat feedback is crucial in igniting the nearby unreacted material and sustaining steady propagation. This accounts for the transition from noncontinuous propagation to steady propagation observed upon the incorporation of carbon fiber into the mesoparticle composite.

3. Conclusion

In this paper, we investigate the combustion characteristics of a free-standing composite consisting of 90 wt% nanoenergetic mesoparticles fabricated via 3D printing. SEM analysis of the printed composite confirms that the integrity of the mesoparticles is maintained during the printing process. High-speed microscopic imaging reveals the expected reduction in sintering for the composite of mesoparticles compared to the physical mixture. However, macroscopic imaging shows noncontinuous and oscillating propagation behavior in the mesoparticle composite, which is attributed to insufficient heat feedback from the flame to the unburnt material. To enhance heat feedback, carbon fiber (C.F.) is incorporated into the composite to intercept agglomerates near the burning surface. With 2 wt% C.F. inclusion, steady propagation of the composite is observed. A theoretical calculation is performed to investigate heat feedback by comparing the residence time and characteristic heat transfer time of agglomerates near the burning surface. The calculation reveals that the overall agglomerate residence time is substantially longer than the heat transfer time for the mesoparticle composite with C.F., while they are of similar magnitude for the composite without C.F., thus confirming the increased heat feedback with C.F. incorporation. This study underscores the critical role of heat feedback in the combustion behavior of energetic composites.

4. Experimental Section

Materials: Aluminum nanoparticles (Al NPs, ≈70 nm, 66 wt% active) were purchased from US Research Nanomaterials Inc. The active content of Al NPs was determined with thermogravimetry and differential scanning calorimetry (TGA–DSC, Netsch STA449 F3 Jupiter).[7,43] Copper oxide nanoparticles (CuO, ≈40 nm) were obtained from U.S. Research Nanomaterials. Polymethyl methacrylate (PMMA, MW = 550000) was purchased from Alfa Aesar and METHOCEL F4M Hydroxypropyl Methylcellulose (HPMC) was obtained from Dow Chemical Company. The Collodion solution (4–8 wt% in ethanol/diethyl ether) was purchased from Sigma–Aldrich, and nitrocellulose (NC) was obtained by drying the collodion solution. Carbon fiber (C.F., diameter: 7 μm, length: ≈3 mm) was purchased from Composite Envisions. Ethanol (200 proof) was purchased from Koptec. Dichloromethane (99.9%), N-dimethylformamide (DMF), 2-propanol (IPA), and acetone (99.5%) were purchased from Fisher Scientific.

Synthesis of Al-CuO-NC Mesoparticles: Details about mesoparticle synthesis can be found in the previous publication.[25] Briefly, Al NPs and CuO NPs at a stoichiometric ratio were added to an NC solution in the mixture of DMF:IPA:acetone (3:5:2 in volume). The choice of 7.5 wt% NC was based on the prior work which showed an optimal result.[25] The suspension was sonicated for 1 h, followed by a minimum of 24 h of stirring. The obtained suspension was spray-dried into mesoparticles with a Büchi B-290 Mini Spray Dryer. Argon preheated at ≈110 °C was used as the drying gas throughout the spray drying system.

3D Printing: Details about 3D printing of 90 wt% loading composites can be found in previous publications from the group.[20,43] Generally, the inks were prepared by first dissolving 10 wt% PMMA or 4 wt% PMMA and 6 wt% HPMC in the mixture of ethanol and dichloromethane (1:1 in volume). Mesoparticles were then added and ultrasonicated for 15 min and magnetically stirred for ≈1 h. For preparing the ink for composite with carbon fiber, 2 wt% was added to the PMMA/HPMC solution and gently stirred for ≈1 h before the addition of mesoparticles. For printing, ink was extruded through a 14-gauge nozzle and written directly on a glass substrate kept at room temperature. The obtained films were then cut into ≈2 cm long free-standing sticks for further characterization. It is noteworthy that while mesoparticles can be printed with both PMMA and PMMA/HPMC as the binder, mesoparticles with carbon fiber can only be printed with PMMA/HPMC. This was because the low viscosity of the PMMA solution leads to the rapid settling of carbon fiber, resulting in a failed print. The solution of PMMA/HPMC has a significantly higher viscosity that ensures successful printing.

Characterizations: A scanning electron microscope (SEM, ThermoFisher Scientific NNS450) was used to characterize the morphology of the as synthesized mesoparticles, printed composites, and post-combustion products.

In Operando Microscopic and Macroscopic Imaging: Details of *in operando* macro and microscopic/pyrometry imaging process can be found in the previous publications.[18,44] Briefly, two color imaging systems were aligned on two opposite sides of a printed stick mounted inside a chamber. One was a macroscopic imaging system with a high-speed camera (Vision Research Phantom Miro M110). The other was a microscopic imaging system with a high-speed camera (Vision Research Phantom VEO710L) coupled with Infinity Photo-Optical Model K2 DistaMax. (The microscopic imaging videos were utilized for measuring temperature with pyrometry, which will be discussed in more detail in the following section.) A coiled nichrome wire connected to a power supply was placed immediately adjacent to one end of the printed stick and Joule-heated to ignition. The combustion process was recorded by both of the imaging systems. It was worth noting that the chamber was filled with air for the composites of physically mixed Al/CuO and mesoparticle with only PMMA as the binder. This was because the composite containing mesoparticles with PMMA failed to propagate in an argon environment. In contrast, the chamber was filled with argon for the composites of mesoparticle with PMMA/HPMC as the binder.

Three-Color Imaging Pyrometry: Details of three-color imaging pyrometry can be found in the previous studies.[18,27,29] Briefly, temperature measurements were performed by analyzing the channel intensity ratios of three colors (red, green, and blue) captured by the Bayer filter of the camera. A custom MATLAB routine was utilized for this analysis with the assumption that the sample exhibited graybody emission behavior. A blackbody source (Mikron M390) was used to obtain calibration factors. The temperature measurement uncertainty was estimated to be nominally 200–300 K.[27,29]

Infrared Radiation (IR) Camera Imaging: IR measurement of the printed mesoparticle with PMMA as the binder was performed with an IR camera (Telops FAST M3K high-speed infrared camera) to capture the infrared radiation signals.

Supporting Information

Supporting Information is available from the Wiley Online Library or from the author.

Acknowledgements

This work was supported by DTRA-MSEE and the Army Research Office.

Conflict of Interest

The authors declare no conflict of interest.

Data Availability Statement

The data that support the findings of this study are available from the corresponding author upon reasonable request.

Keywords

assembly, combustion, heat transfer, mesoparticle, propagation

Received: April 19, 2024
Revised: June 6, 2024
Published online: July 29, 2024

[1] G. C. Egan, K. T. Sullivan, T. Y. Olson, T. Y.-J. Han, M. A. Worsley, M. R. Zachariah, *J. Phys. Chem. C* **2016**, *120*, 29023.
[2] D. Sundaram, V. Yang, R. A. Yetter, *Prog. Energy Combust. Sci.* **2017**, *61*, 293.
[3] M. Comet, C. Martin, F. Schnell, D. Spitzer, *Propellants Explos. Pyrotech.* **2019**, *44*, 18.
[4] N. Zohari, M. H. Keshavarz, S. A. Seyedsadjadi, *Cent. Eur. J. Energ. Mater.* **2013**, *10*.
[5] R. A. Yetter, G. A. Risha, S. F. Son, *Proc. Combust. Inst.* **2009**, *32*, 1819.
[6] B. W. Asay, S. F. Son, J. R. Busse, D. M. Oschwald, *Propellants Explos. Pyrotech.* **2004**, *29*, 216.
[7] K. Sullivan, G. Young, M. R. Zachariah, *Combust. Flame* **2009**, *156*, 302.
[8] K. T. Sullivan, J. D. Kuntz, A. E. Gash, *Propellants Explos. Pyrotech.* **2014**, *39*, 407.
[9] M. R. Weismiller, J. Y. Malchi, J. G. Lee, R. A. Yetter, T. J. Foley, *Proc. Combust. Inst.* **2011**, *33*, 1989.
[10] T. R. Sippel, S. F. Son, L. J. Groven, *Combust. Flame* **2014**, *161*, 311.
[11] H. Wang, Y. Wang, M. Garg, J. S. Moore, M. R. Zachariah, *Combust. Flame* **2022**, *244*, 112242.
[12] L. T. DeLuca, L. Galfetti, G. Colombo, F. Maggi, A. Bandera, V. A. Babuk, V. P. Sinditskii, *J. Propuls. Power* **2010**, *26*, 724.
[13] R. J. Jacob, B. Wei, M. R. Zachariah, *Combust. Flame* **2016**, *167*, 472.
[14] P. Chakraborty, M. R. Zachariah, *Combust. Flame* **2014**, *161*, 1408.
[15] M. R. Zachariah, M. J. Carrier, *J. Aerosol Sci.* **1999**, *30*, 1139.
[16] R. A. Yetter, *Proc. Combust. Inst* **2021**, *38*, 57.
[17] E. L. Dreizin, *Prog. Energy Combust. Sci.* **2009**, *35*, 141.
[18] H. Wang, D. J. Kline, M. R. Zachariah, *Nat. Commun.* **2019**, *10*, 3032.
[19] Y. Wang, G. I. Paul, E. Hagen, H. Wang, M. R. Zachariah, *Combust. Flame* **2024**, *262*, 113373.
[20] Y. Wang, E. Hagen, P. Biswas, H. Wang, M. R. Zachariah, *Combust. Flame* **2023**, *252*, 112747.
[21] G. C. Egan, K. T. Sullivan, T. LaGrange, B. W. Reed, M. R. Zachariah, *J. Appl. Phys.* **2014**, *115*, 084903.
[22] K. T. Sullivan, N. W. Piekiel, C. Wu, S. Chowdhury, S. T. Kelly, T. C. Hufnagel, K. Fezzaa, M. R. Zachariah, *Combust. Flame* **2012**, *159*, 2.
[23] H. Wang, G. Jian, G. C. Egan, M. R. Zachariah, *Combust. Flame* **2014**, *161*, 2203.
[24] H. Wang, R. J. Jacob, J. B. DeLisio, M. R. Zachariah, *Combust. Flame* **2017**, *180*, 175.
[25] M. Chowdhury, P. Ghildiyal, A. Rojas, Y. Wang, H. Wang, M. R. Zachariah, *Adv. Powder Technol.* **2023**, *34*, 104075.
[26] G. Young, H. Wang, M. R. Zachariah, *Propellants Explos. Pyrotech.* **2015**, *40*, 413.
[27] H. Wang, D. J. Kline, M. C. Rehwoldt, M. R. Zachariah, *ACS Appl. Mater. Interfaces* **2021**, *13*, 30504.
[28] H. Wang, E. Hagen, K. Shi, S. Herrera, F. Xu, M. R. Zachariah, *Chem. Eng. J.* **2023**, 141653.
[29] D. J. Kline, Z. Alibay, M. C. Rehwoldt, A. Idrogo-Lam, S. G. Hamilton, P. Biswas, F. Xu, M. R. Zachariah, *Combust. Flame* **2020**, *215*, 417.
[30] A. Ishihara, M. Q. Brewster, T. A. Sheridan, H. Krier, *Combust. Flame* **1991**, *84*, 141.
[31] M. Q. Brewster, B. E. Hardt, *J. Propuls. Power* **1991**, *7*, 1076.
[32] G. C. Egan, M. R. Zachariah, *Combust. Flame* **2015**, *162*, 2959.
[33] M. Summerfield, *Solid Propellant Rocket Research*, Elsevier, Amsterdam, **2013**.
[34] M. Zarzecki, J. G. Quintiere, R. E. Lyon, T. Rossmann, F. J. Diez, *Combust. Flame* **2013**, *160*, 1519.
[35] C. W. M. Van Der Geld, P. A. O. G. Korting, T. Wijchers, *Combust. Flame* **1990**, *79*, 299.
[36] C. A. Kramer, R. Loloee, I. S. Wichman, R. N. Ghosh, *American Society Of Mechanical Engineers Digital Collection* **2010**, 99.
[37] R. N. Ghosh, I. S. Wichman, C. A. Kramer, R. Loloee, *Fire Mater.* **2013**, *37*, 280.

[38] T. Cai, G. Wang, W. Zhang, X. Gao, *Measurement* **2012**, *45*, 2089.
[39] G. Fu, D. K. Sing, J. D. Lothringer, D. Deming, J. Ih, E. M.-R. Kempton, M. Malik, T. D. Komacek, M. Mansfield, J. L. Bean, *Astrophys. J. Lett.* **2022**, *925*, L3.
[40] Y. Zhou, M. R. Zachariah, *Energy Fuels* **2024**, *38*, 8992.
[41] W. M. Rohsenow, J. P. Hartnett, E. N. Ganic, **1985**.
[42] Y. Wang, H. Wang, F. Xu, P. Ghildiyal, M. R. Zachariah, *Chem. Eng. J.* **2022**, *446*, 136786.
[43] H. Wang, J. Shen, D. J. Kline, N. Eckman, N. R. Agrawal, T. Wu, P. Wang, M. R. Zachariah, *Adv. Mater.* **2019**, *31*, 1806575.
[44] H. Wang, B. Julien, D. Kline, Z. Alibay, M. Rehwoldt, C. Rossi, M. Zachariah, *J. Phys. Chem. C* **2020**, *124*, 13679.